International Journal of Heat and Mass Transfer 52 (2009) 5358–5370

Contents lists available at ScienceDirect

International Journal of Heat and Mass Transfer

journal homepage: www.elsevier.com/locate/ijhmt

Fluid flow and heat transfer characteristics of cross-cut heat sinks

Tae Young Kim, Sung Jin Kim *

School of Mechanical, Aerospace and Systems Engineering, Korea Advanced Institute of Science and Technology, Daejeon 305-701, Republic of Korea

ARTICLE INFO

Article history:
Received 23 September 2008
Received in revised form 3 July 2009
Accepted 3 July 2009
Available online 18 August 2009

Keywords:
Cross-cut heat sink
Thermal optimization

ABSTRACT

In this study, effects of cross-cuts on the thermal performance of heat sinks under the parallel flow condition are experimentally studied. To find effects of the length, position, and number of cross-cuts, heat sinks with one or several cross-cuts ranging from 0.5 mm to 10 mm were fabricated. The pressure drop and the thermal resistance of the heat sinks are obtained in the range of 0.01 W$<P_p<$ 1 W. Experimental results show that among the many cross-cut design parameters, the cross-cut length has the most significant influence on the thermal performance of heat sinks. The results also show that heat sinks with a cross-cut are superior to heat sinks containing several cross-cuts in the thermal performance. Based on experimental results, the friction factor and Nusselt number correlations for heat sinks with a cross-cut are suggested. Using the proposed correlations, thermal performances of cross-cut heat sinks are compared to those of optimized plate-fin and square pin-fin heat sinks under the constant pumping power condition. This comparison yields a contour map that suggests an optimum type of heat sink under the constraint of the fixed pumping power and fixed heat sink volume. The contour map shows that an optimized cross-cut heat sink outperforms optimized plate-fin and square pin-fin heat sinks when $0.04 < \log L^* < 1$.

1. Introduction

Finned heat sinks are most widely used as a thermal solution to ensure the reliability of electronic devices [1,2] with ever increasing power dissipation and circuit density [3,4]. Since Tuckerman and Pease [5] first introduced the microchannel heat sink, many researchers have studied the thermal characteristics of heat sinks and reported optimum geometries of heat sinks [6–8]. Porous-channel heat sinks or heat sinks combined with porous structures have been also suggested to improve the thermal performance of heat sinks [9–11]. Among various types of heat sinks, plate-fin and pin-fin heat sinks are widely used owing to their own advantages. The plate-fin heat sink has the advantages of a small pressure drop, a simple design and an easy fabrication. On the other hand, the pin-fin heat sink has the advantages of a high heat transfer rate due to the redeveloping regions and an even thermal performance independent of the direction of the fluid flow [12,13]. Recently, Kim et al. [14] revealed that the effective heat sink type between plate-fin and pin-fin heat sinks could be determined depending on the pumping power and heat sink length.

In addition to above research activities, there has been a new attempt to combine the advantages of plate-fin and pin-fin heat sinks [15]. Usually, these types of heat sinks have several cuts, termed cross-cuts in the present study, perpendicular to the direction of the fluid flow. Xu et al. [16] demonstrated a new silicon microchannel heat sink composed of longitudinal microchannels and several transverse microchannels that divide the entire flow path into several independent zones. Experiments for strip-fin heat sinks were performed and empirical correlations were proposed to predict the Nusselt number and pressure drop [17,18]. Noda et al. [19] performed numerical simulations of heat sinks with a cut-fin shape to clarify the effect of a transverse cut on the thermal performance of the heat sinks. Amon et al. [20,21] studied the fluid flow and heat transfer characteristics in communicating channels that have geometry similar to that of cross-cut heat sinks. The authors of these works found that heat sinks with one or several cross-cuts show better thermal performance than conventional plate-fin or the pin-fin heat sinks. However, they did not quantify the effects of major design parameters, such as the length, position and number of cross-cuts, on the thermal performance of a heat sink.

A main purpose of the present study is to quantify effects of cross-cuts. To this end, an experimental investigation is performed with heat sinks with one or more cross-cuts ranging from 0.5 mm to 10 mm. Cross-cuts of various lengths are made in different positions in heat sinks to identify the most significant design parameter of the cross-cut from among the length, position, and number of cross-cuts. For the purpose of predicting the pressure drop and thermal resistance, respective correlations of the friction factor and Nusselt number for single-cross-cut heat sinks

* Corresponding author. Tel.: +82 42 350 3043; fax: +82 42 350 8207.
E-mail address: sungjinkim@kaist.ac.kr (S.J. Kim).

0017-9310/$ - see front matter © 2009 Elsevier Ltd. All rights reserved.
doi:10.1016/j.ijheatmasstransfer.2009.07.008

Nomenclature

A	wetted surface area (m^2)
A_{fr}	frontal area of the heat sink (m^2) ($\equiv H_f \times W$)
c_p	specific heat (J/kg K)
D_h	hydraulic diameter, m ($\equiv 2Hw_c/(H+w_c)$)
$D_{h,fr}$	hydraulic diameter of frontal area (m) ($\equiv 2HW/(H+W)$)
h	heat transfer coefficient (W/m^2 K)
H	height of the heat sink, m ($\equiv H_f + H_b$)
k	thermal conductivity (W/m K)
L	length of the heat sink (m)
Nu	Nusselt number
n	number of cross-cuts
ΔP	pressure drop across a heat sink (Pa)
P_p	pumping power (W)
Pr	Prandtl number
R	thermal resistance (K/W)
Re_{D_h}	Reynolds number ($\equiv \frac{\rho U D_h}{\mu}$)
T	temperature (K)
V	approach velocity (m/s)
W	heat sink width (m)
w_c	channel width (m)
w_w	fin thickness (m)
x, y, z	Cartesian coordinate

Greek symbols

η	fin efficiency
ρ	density (kg/m^3)
ε	porosity ($\equiv w_c/(w_c+w_w)$)

Subscripts

bm	bulk mean
c	cross-cut
fin	fin
in	inlet
l	from the leading edge
max	maximum
pin	pin-fin heat sink
plate	plate-fin heat sink
w	wall

Superscript

*	dimensionless variables

are proposed based on the experimental results. Through the use of these correlations, design parameters that maximize the thermal performance of cross-cut heat sinks under given conditions of the pumping power and the length of a heat sink could be obtained. Through the optimization process, the thermal performances of three types of heat sinks, a plate-fin heat sink, a square pin-fin heat sink, and a cross-cut heat sink, are compared under the constraint of a fixed pumping power and a fixed heat sink volume. Finally, a contour map that shows the optimum type of heat sink as a function of the dimensionless pumping power and heat sink length is obtained.

2. Experimental setup and procedure

Thirty-three heat sinks made of aluminum alloy 6061 (k = 171 W/m K) were fabricated using a wire cutting technique. The configurations and detailed dimensions of these heat sinks are presented in Fig. 1 and Table 1, respectively. The height of the heat sink base (H_b) tested in the present study is 6 mm. In this paper, a heat sink with a single cross-cut is termed a single-cross-cut heat sink and a heat sink with several cross-cuts is termed a multiple-cross-cut heat sink for convenience. A schematic diagram of the experimental apparatus is shown in Fig. 2. The wind tunnel duct consists of acrylic plates of a thickness of 9.1 mm. The width and height of the wind tunnel duct are 50 mm and 30 mm, respectively. A thin film heater fabricated using Kapton-coated stainless steel of a thickness of 0.25 μm is attached to the bottom surface of a heat sink. It plays the role of a heat source as it is connected to a DC power supply (E3632A, Agilent). To reduce heat loss, a Bakelite plate (k = 0.23 W/m K) with 10 mm thickness is attached to the bottom surface of the thin film heater. The Bakelite plate is then attached to the bottom of the wind tunnel duct using six screws. Installation of the heat sink into the wind tunnel duct is shown in Fig. 3. There is no clearance between the wind tunnel duct and the top of the heat sink, while there exists half channel width between the fins and the two sides of the wind tunnel duct. The heat sink base is flush with the bottom wall of the wind tunnel duct. A honeycomb is positioned 50 mm in front of the heat sink to ensure a uniform flow profile. There are 11 pressure taps at the top wall of the wind tunnel duct to measure the pressure drop across the heat sink along the air flow direction. The spacing between any two adjacent pressure taps is 10 mm. The first pressure tap is located 20 mm upstream of the heat sink and the last one is located 20 mm downstream of the heat sink. The pressure drop across the heat sink is the difference of the pressures measured at the first and the last pressure taps. The air volume flow rate through the wind tunnel duct and the pressure drop across the heat sink are measured using a laminar flow element and a micro-manometer (Furness-Controls Ltd.), respectively. The uncertainty of the laminar flow element is ±1%, and the full range and uncertainty of the micro-manometer are 200 Pa and ±0.056%, respectively. By measuring the volume flow rate $\dot{Q}$ and the pressure drop across the heat sink ΔP, the pumping power can be calculated from the following equation:

$$P_p = \dot{Q} \times \Delta P \tag{1}$$

Nineteen J-type thermocouples were used for temperature measurement. To measure the maximum temperature of the heat sink, nine thermocouples were mounted through 5 mm deep holes at the base plate of the heat sink, which are positioned along the centerline of the heat sink. They are 6 mm apart. The first thermocouple is positioned 6 mm from the leading edge of the heat sink and the last one is positioned 6 mm from the end of the heat sink. One thermocouple was used to measure the inlet temperature. To measure the heat loss another nine thermocouples were attached to the Bakelite plate and the inner surface and outer surface of the wind tunnel duct. The uncertainty of each thermocouple is approximately 0.75%. A HP 34970A data acquisition unit is utilized to convert the electrical signals measured by the thermocouples into temperature information.

The test procedures were as follows: the desired volume flow rate of the air was generated by a suction-type blower and its value was obtained by the laminar flow element. The heater was then powered up to a heat load of 60 W and was allowed to stabilize. The heat load was calculated by multiplying the current and the voltage drop through the heater. The measured heat losses in the experiments were in the range of 3–7% of the heat load supplied by the heater. Once the heat load was fixed, the base temperature of the heat sink was monitored. A steady-state

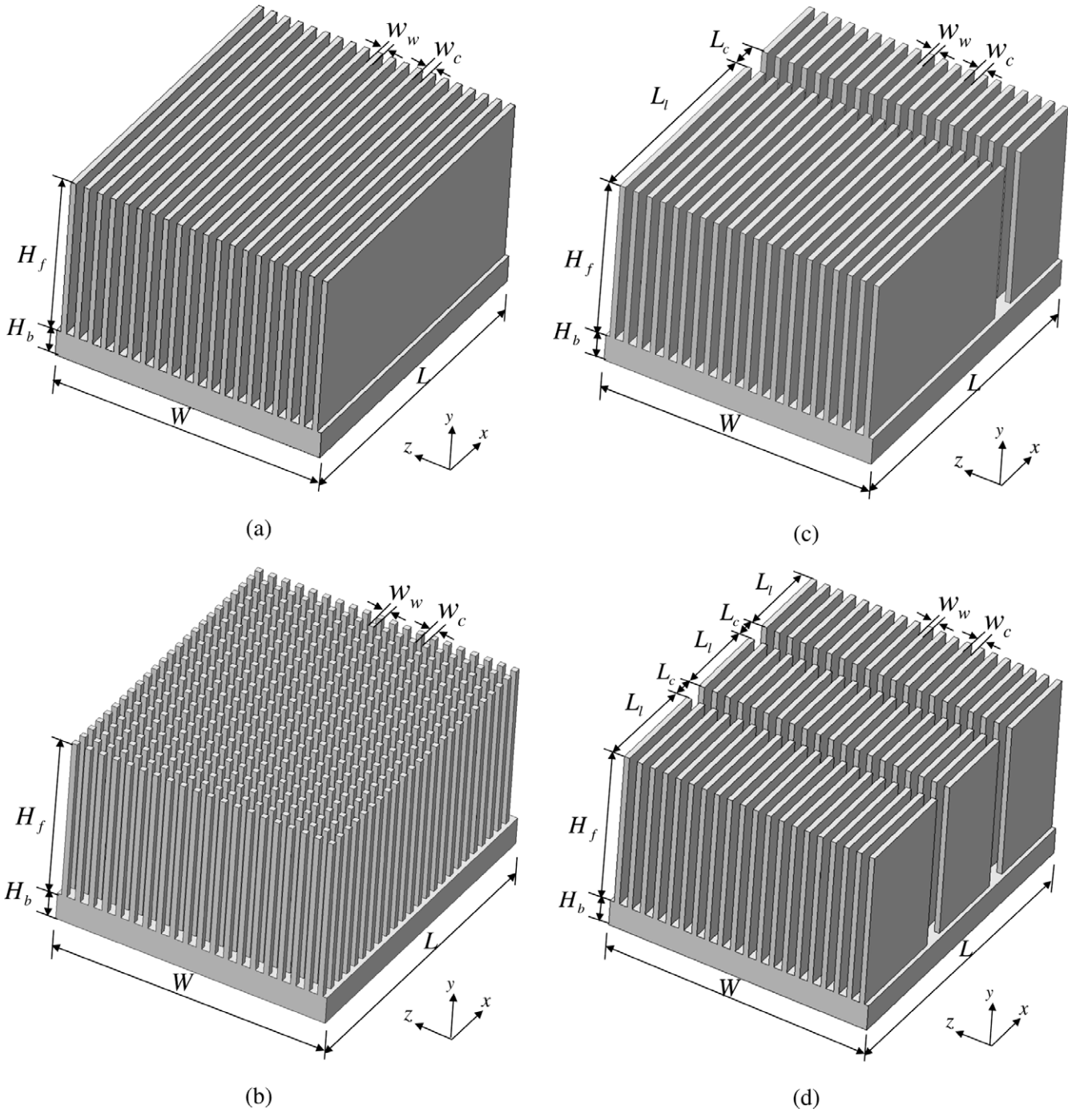

Fig. 1. The configuration of the tested heat sinks. (a) Plate-fin heat sink, (b) square pin-fin heat sink, (c) single-cross-cut heat sink and (d) multiple-cross-cut heat sink ($n = 2$).

was assumed when the change in the maximum temperature of the heat sink was smaller than ±0.1 °C for a period of 2 min. The maximum base temperature of the heat sink and the bulk mean inlet temperature were used to calculate the thermal resistance of the heat sink,

$$R = \frac{T_{w,max} - T_{bm,in}}{q} \tag{2}$$

The actual heat flow rate from the heater to the heat sink was calculated by subtracting the heat loss from the heat load supplied by the heater. The uncertainties shown by the error bars in the experimental results include both the random error and the systematic error, as described in Ref. [22].

3. Results and discussion

3.1. Validation

To check the validity of the present study, the experimental results of the pressure drop and thermal resistance of a plate-fin heat sink, one of the experimental cases, were compared to those obtained from existing correlations. Fig. 4(a) shows that the experimental results of the pressure drop are in good agreement with

Table 1
Dimensions of tested heat sinks. Unit: mm.

Cross-cut heat sinks				
Heat sink width, W	Heat sink length, L		Fin height, H_f	Fin thickness, w_w
Fixed design parameters				
50	60		30	1
Channel width, w_c	Number of cross-cuts, n		Cross-cut position, L_l	Length of cross-cuts, L_c
Varying design parameters				
1	1		20	1, 2.5, 5, 7
			40	1, 2.5, 5, 7
1.5	1		20	0.5, 1, 2.5, 5, 10
			40	0.5, 1, 2.5, 5, 10
	2		Equally spaced	1, 5, 10
	3		Equally spaced	1, 2.5, 5
2	1		20	1
			40	1
	5		Equally spaced	1
2.5	1		20	1
			40	1
Heat sink width, W	Heat sink length, L	Fin height, H_f	Fin thickness, w_w	Channel width, w_c
Plate-fin heat sink				
50	60	30	1	1.5
Square pin-fin heat sink				
50	60	30	1	1.5

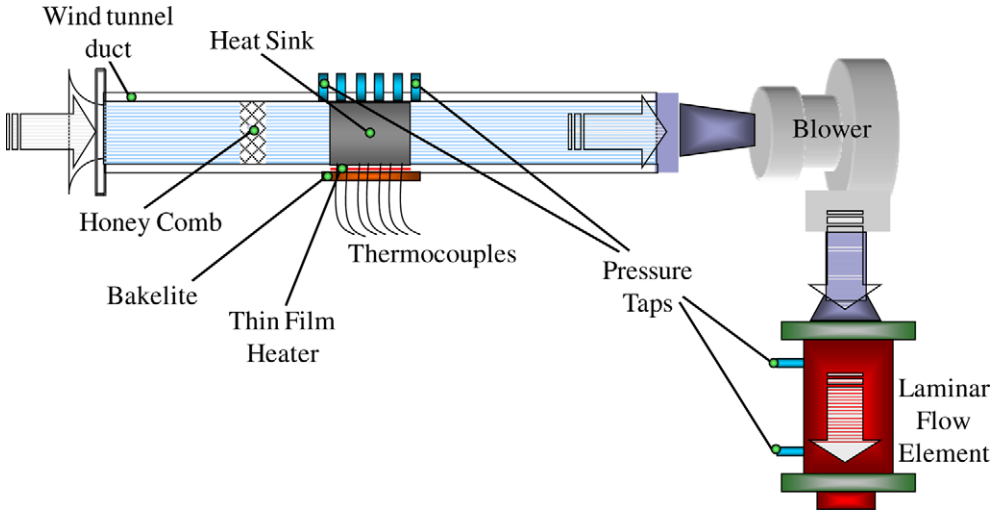

Fig. 2. Schematic diagram of the experimental apparatus.

the correlation suggested by Muzychka and Yovanovich [23] within 4% error. In addition, as shown in Fig. 4(b), experimental results of the thermal resistance also correspond well to the correlation proposed by Teertstra et al. [24] within 6.8% error. Based on these comparisons, it is clear that the experiments in this study were properly conducted.

3.2. Parametric studies

3.2.1. Effects of the cross-cut length

In this section, effects of the cross-cut length are presented for single-cross-cut heat sinks with one cross-cut positioned 40 mm from the leading edge (L_1 = 40 mm in Fig. 1(c)).

Fig. 5 shows the approach velocity ratios of cross-cut heat sinks and an equivalent plate-fin heat sink with design parameters that are identical to those of the cross-cut heat sinks, apart from the cross-cut region. As the pumping power increases, the approach velocity ratio decreases. This implies that as the pumping power increases, an additional pressure drop generated in the cross-cut region increases due to the flow separation [14], the higher skin friction associated with the boundary layer restarting [20], and the form drag caused by the structural change of the fins [25]. If the length of the cross-cut considerably increases, the total pressure drop would be reduced due to the decreased friction loss at the fin surface, even when an additional pressure drop is generated in the cross-cut region. As a result when the dimensionless cross-cut length, L_c^* ($\equiv L_c/L$), is larger than 0.0833 (i.e., $L_c > 5$ mm with L = 60 mm) the approach velocity ratios increase as the length of the cross-cut increases.

When P_p = 0.01 W, the value of the approach velocity ratio is greater than 1. This is because when the pumping power is small, the pressure drop of the cross-cut heat sink is smaller than that of

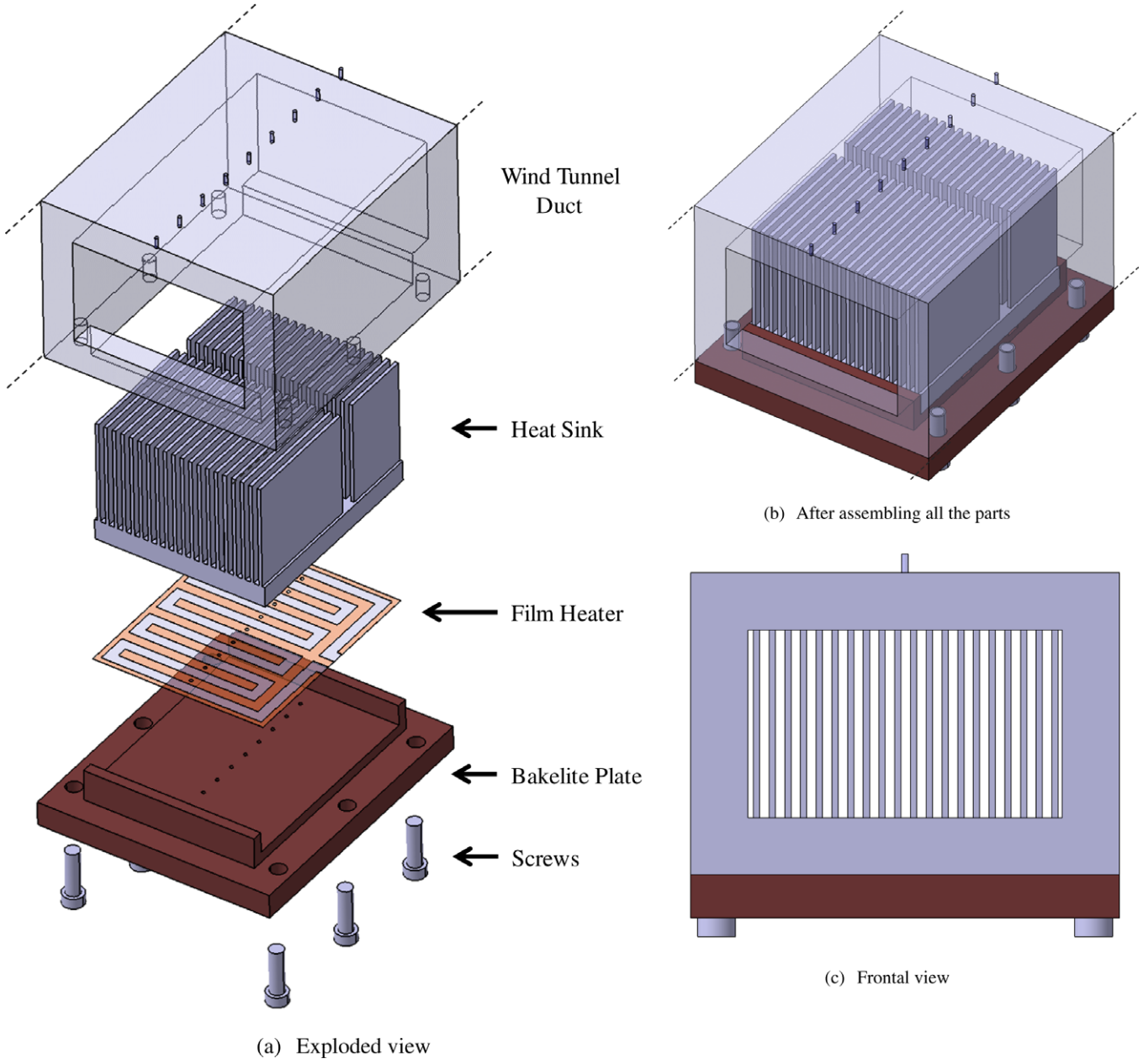

Fig. 3. Installation of the heat sink into the wind tunnel duct.

the equivalent plate-fin heat sink. In this case the approach velocity is small, which makes the additional pressure drop, caused by flow separation and secondary flow effects in the cross-cut region negligible [16]. On the other hand, in the cross-cut region, there is no skin friction generated by the interaction between the fluid flow and the fin surface.

In Fig. 6, the thermal resistances of cross-cut heat sinks are compared to those of equivalent plate-fin and square pin-fin heat sinks under the constant pumping power condition. In order to verify the effect of the cross-cut length, the other parameters of the three types of heat sinks, in this case the fin thickness, channel width and size, were equalized, as presented in Table 1. As shown in Fig. 6(a), cross-cut heat sinks perform better than the equivalent plate-fin heat sink in most experimental ranges. In the best cases, cross-cut heat sinks show better thermal performance by 5–18% compared to the equivalent plate-fin heat sink. The improvement in the thermal performance of cross-cut heat sinks becomes greater as the pumping power increases in spite of poor flow characteristics of cross-cut heat sinks in high pumping power regions. This implies that the advantage of heat transfer enhancement caused by the cross-cut far outweighs the disadvantage of the pressure drop increment. However, when $L_c^* = 0.1667$ ($L_c = 10$ mm), the thermal performance of the heat sink decreases due to the small heat transfer area.

As shown in Fig. 6(b), cross-cut heat sinks perform better by approximately 14–16% compared to the equivalent square pin-fin heat sink in the best cases. In contrast to that shown in Fig. 6(a), as the pumping power increases, the thermal performance of the cross-cut heat sinks is reduced by less than that of the equivalent pin-fin heat sink. This result is similar to the results in an earlier study [14]. Based on Fig. 6(a) and (b), the

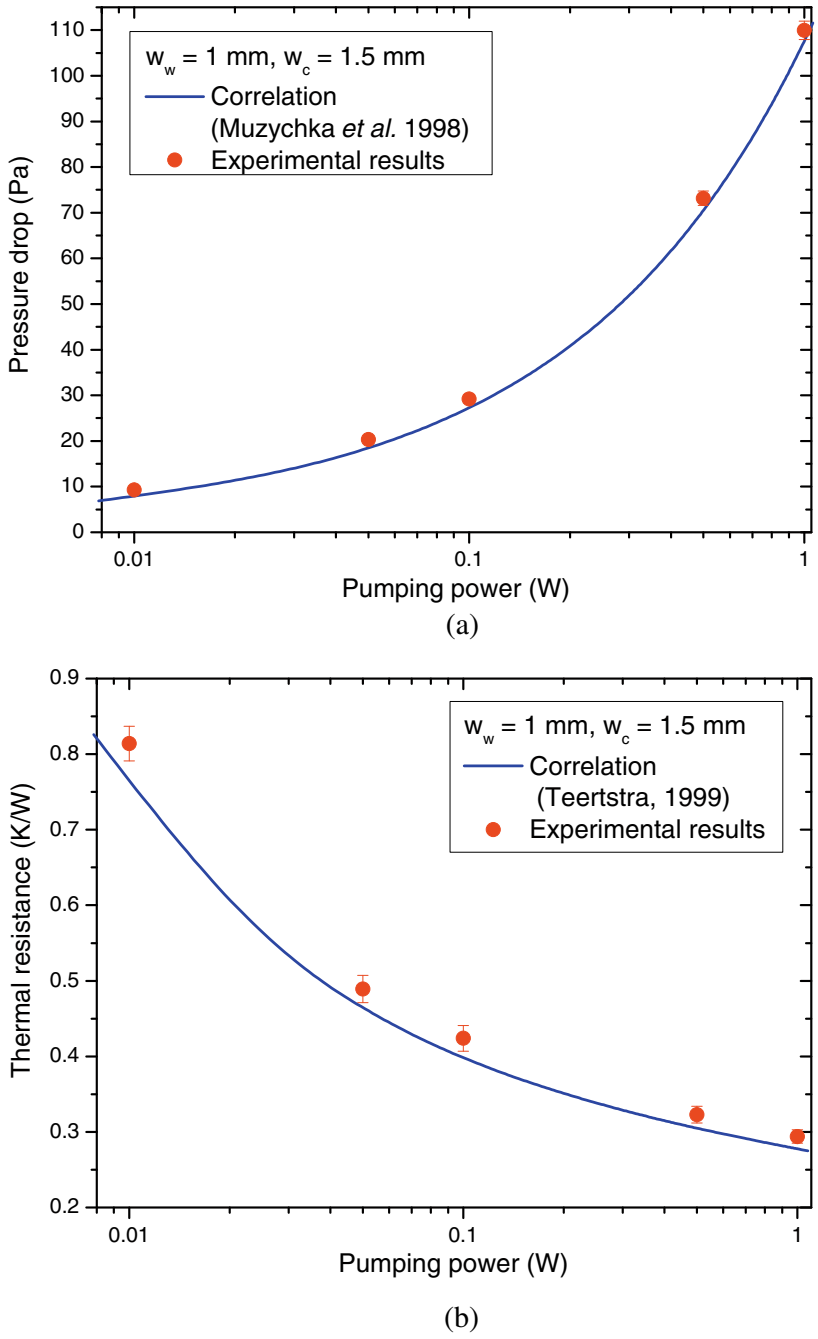

Fig. 4. Validation of the experimental results. (a) Pressure drop and (b) thermal resistance.

optimum cross-cut length is shown to exist at approximately 5 mm when the ratio of the channel width to the fin pitch (ε) is 0.6.

3.2.2. Effects of the cross-cut position

There are also open questions as to how much the position of the cross-cut affects the thermal performance of a heat sink and where the cross-cut should be positioned on the heat sink to improve the thermal performance. In this section, the thermal performances of different heat sinks, each of which has a cross-cut in a different position relative to the leading edge of the heat sink, are compared. In this comparison, $L_l = 20$ mm and $L_l = 40$ mm; these values imply that the cross-cut is positioned 20 mm and 40 mm, respectively, from the leading edge of the heat sink. These values were selected as the cross-cut positions. Fig. 7(a) and (b) shows that heat sinks with a cross-cut at $L_l = 40$ mm show slightly better thermal performance compared to when $L_l = 20$ mm. However, the cross-cut position is not an important parameter because change of the thermal resistance value only ranges from 1% to 3.5% according to the cross-cut position.

3.2.3. Effects of the number of cross-cuts

In order to verify effects of the number of cross-cuts, multiple-cross-cut heat sinks with several cross-cuts were also fabricated and their fluid flow and heat transfer characteristics were experimentally investigated. In the case of multiple-cross-cut heat sinks, the cross-cuts are parallel to each other and are equally spaced on the heat sink, as shown in Fig. 1(d). Fig. 8 shows effects of the number of cross-cuts on thermal resistance.

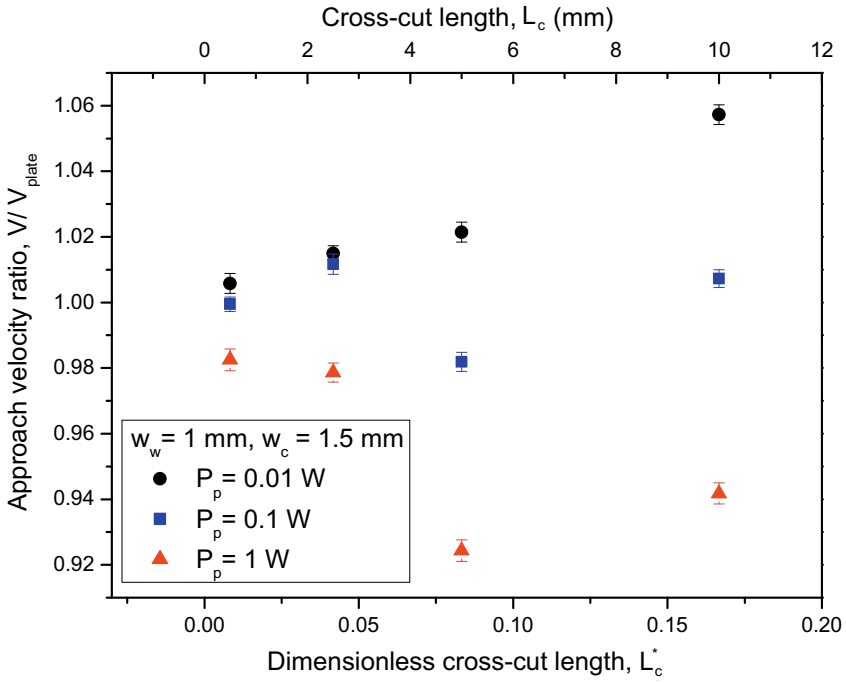

Fig. 5. Approach velocity ratio of cross-cut heat sinks to the plate-fin heat sink.

The thermal resistance of a heat sink is strongly affected by the number of cross-cuts, especially in a large pumping power region. The thermal performance of heat sinks varies according to the number of cross-cuts up to nearly 22% and 30% according to Fig. 8(a) and (b). However, it is important to note that single-cross-cut heat sinks are superior to multiple-cross-cut heat sinks in terms of thermal performance regardless of the pumping power when they are subject to a parallel flow. This is because the disadvantage of the pressure drop increment far outweighs the advantage of heat transfer improvement by the thermal boundary layer redevelopment, as the number of cross-cuts increases. In addition, the heat transfer area reduction due to the cross-cutting becomes significant for multiple-cross-cut heat sinks as the number of cross-cuts increases. Because experimental results are somewhat limited, more detailed study is necessary to quantify the effects of the number of cross-cuts on the thermal performance of heat sinks.

3.3. Correlations

As presented in the previous section, single-cross-cut heat sinks outperform multiple-cross-cut heat sinks. However, the fluid flow and heat transfer characteristics of cross-cut heat sinks are affected by various design parameters and cannot be easily predicted through an analytical approach. For this reason, correlations for predicting the friction factor and the Nusselt number of single-cross-cut heat sinks are suggested in this section based on experimental results. To determine the correlations, it was recalled that single-cross-cut heat sinks are similar in shape to plate-fin heat sinks except for the cross-cut region. Therefore, correlations for single-cross-cut heat sinks were developed by adding the empirical coefficients that account for the effect of a cross-cut to existing semi-empirical correlations for plate-fin heat sinks. The friction factor correlation suggested by Muzychka and Yovanovich [23] and the Nusselt number correlation proposed by Teertstra et al. [24] for plate-fin heat sinks were used as basic forms as they accurately predict the experimental results for plate-fin heat sinks, as shown in Fig. 4. Because the empirical coefficients in the correlations are expressed as a function of the porosity ε and the dimensionless cross-cut length L_c^*, the proposed correlations are generally applicable, regardless of the heat sink length, the channel width and the fin thickness.

3.3.1. The friction factor correlation

The friction factors for parallel plates are suitably reported in the composite model form of the two limiting cases involving hydrodynamically developing and fully developed flows [23]. These two limiting cases were used as asymptotic solutions for the cases of a small and a large Reynolds number. By adding empirical coefficients α and β to the existing friction factor correlation for plate-fin heat sinks, a friction factor correlation for cross-cut heat sinks is obtained, as shown below.

$$f_{\mathrm{app}}Re_{D_h} = \left[\left(\frac{3.44}{\sqrt{L^+}}\right)^{2+\alpha} + (fRe_{D_h})^{2+\beta}\right]^{\frac{1}{2}} \tag{3}$$

Here,

$$L^+ = \frac{L}{D_h Re_{D_h}},$$

$$fRe_{D_h} = 24 - 32.527\left(\frac{w_c}{H}\right) + 46.721\left(\frac{w_c}{H}\right)^2 - 40.829\left(\frac{w_c}{H}\right)^3 + 22.954\left(\frac{w_c}{H}\right)^4 - 6.089\left(\frac{w_c}{H}\right)^5 \tag{4}$$

The Reynolds number based on the hydraulic diameter of the heat sink channel ($\equiv 2w_c$) is in the range of 250–2350 for which the flow between the two adjacent fins of the heat sink is laminar [26]. The coefficients α and β account for the hydrodynamic effect of a cross-cut on the developing region and fully developed regions,

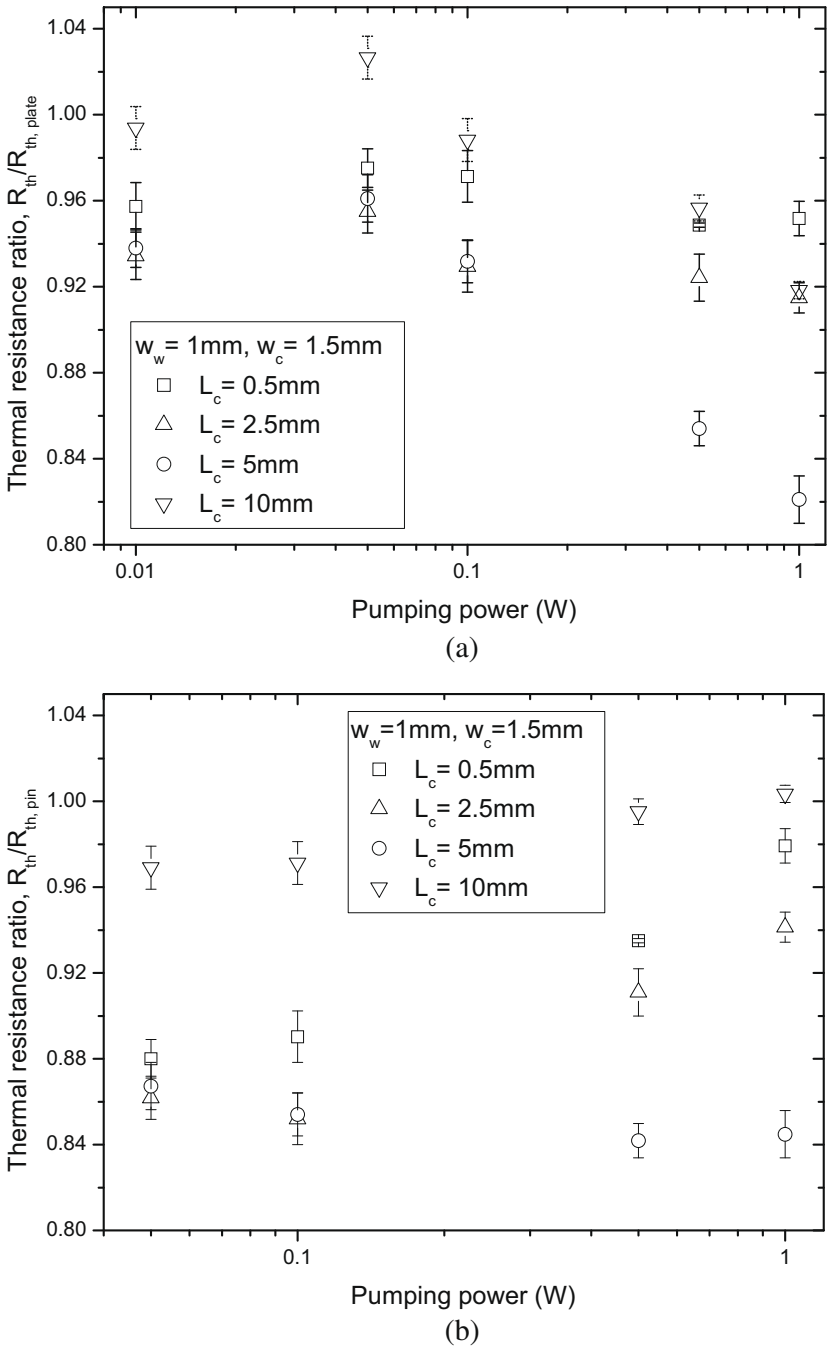

Fig. 6. Thermal resistance ratios: (a) cross-cut heat sinks to the plate-fin heat sink and (b) cross-cut heat sinks to the square pin-fin heat sink.

respectively. The values of α and β are determined from the experimental results. They are given as

$$\alpha = L_c^*\varepsilon(88 - 304\varepsilon + 267\varepsilon^2)\exp\left[-0.5\left(\frac{L_c^* - (0.1 - 0.06\varepsilon)}{-0.12 + 0.32\varepsilon}\right)^2\right] \quad (5)$$

$$\beta = L_c^*\left\{(0.1 + 0.4\varepsilon) + (170 - 621\varepsilon + 533\varepsilon^2) \times \exp\left[-0.5\left(\frac{L_c^* - (0.06 + 0.11\varepsilon)}{-0.01 + 0.09\varepsilon}\right)^2\right]\right\} \quad (6)$$

Fig. 9 shows that the proposed friction factor correlation for single-cross-cut heat sinks predicts the experimental results well. The two dotted lines represent ±20% deviation from the suggested correlation.

3.3.2. The Nusselt number correlation

A Nusselt number correlation for cross-cut heat sinks was also developed based on the composite model of the two limiting cases of thermally developing and fully developed flows. By adding empirical coefficients γ and δ to the Nusselt number correlation for plate-fin heats, as proposed in Ref. [24], the Nusselt number correlation for cross-cut heat sinks is given as

$$Nu = \frac{hD_h}{k_f} = \left[Nu_g^{n+\gamma} + Nu_d^{n+\delta}\right]^{\frac{1}{n}} \quad (7)$$

where

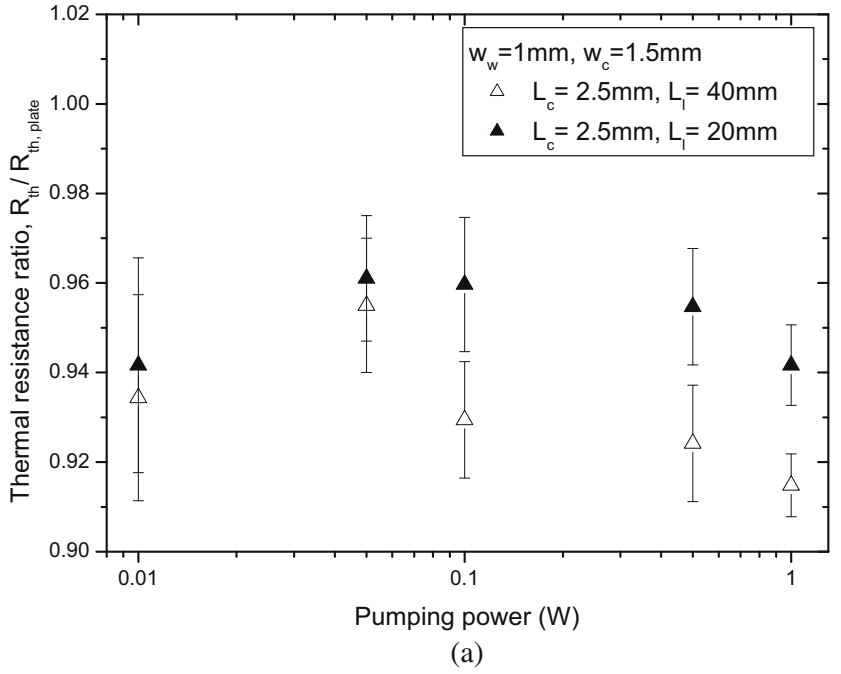

Fig. 7. The effect of the position of the cross-cut on the thermal performance of heat sinks: (a) a length of cross-cut = 2.5 mm and (b) a length of cross-cut = 5 mm.

$$Nu_g = 0.664\sqrt{Re^*_{w_c}}Pr^{1/3}\sqrt{1+\frac{3.65}{\sqrt{Re^*_{w_c}}}},$$
$$Nu_d = \frac{1}{2}Re^*_{w_c}Pr, \quad Re^*_{w_c} = Re_{w_c}\left(\frac{w_c}{L}\right), \quad n=-3 \tag{8}$$

The two terms Nu_g and Nu_d on the right side of Eq. (7) are the asymptotic solutions of the Nusselt number for thermally developing and fully developed flows in parallel plates, respectively. The empirical coefficients γ and δ imply the thermal effects of a cross-cut on the developing and fully developed regions, respectively.

$$\gamma = L^*_c(399-1254\varepsilon+971\varepsilon^2)(-955+3500\varepsilon-3140\varepsilon^2) \times \exp\left[-0.5\left(\frac{L^*_c-(3.6-11.3\varepsilon+8.5\varepsilon^2)}{-2.2+7.4\varepsilon-5.8\varepsilon^2}\right)^2\right] \tag{9}$$

$$\delta = L^*_c(26-82\varepsilon+65\varepsilon^2)\left\{(-292+958\varepsilon-772\varepsilon^2) + (498-1680\varepsilon+1387\varepsilon^2)\exp\left[-0.5\left(\frac{L^*_c-(2.7-8.8\varepsilon+7.3\varepsilon^2)}{-0.55+1.97\varepsilon-1.6\varepsilon^2}\right)^2\right]\right\} \tag{10}$$

For single-cross-cut heat sinks, the thermal resistance is given as

$$R = \frac{1}{h(A_b+\eta A_{\text{fin}})} \tag{11}$$

The experimental results of the thermal resistance of single-cross-cut heat sinks are well reproduced by the proposed Nusselt number correlation, as shown in Fig. 10.

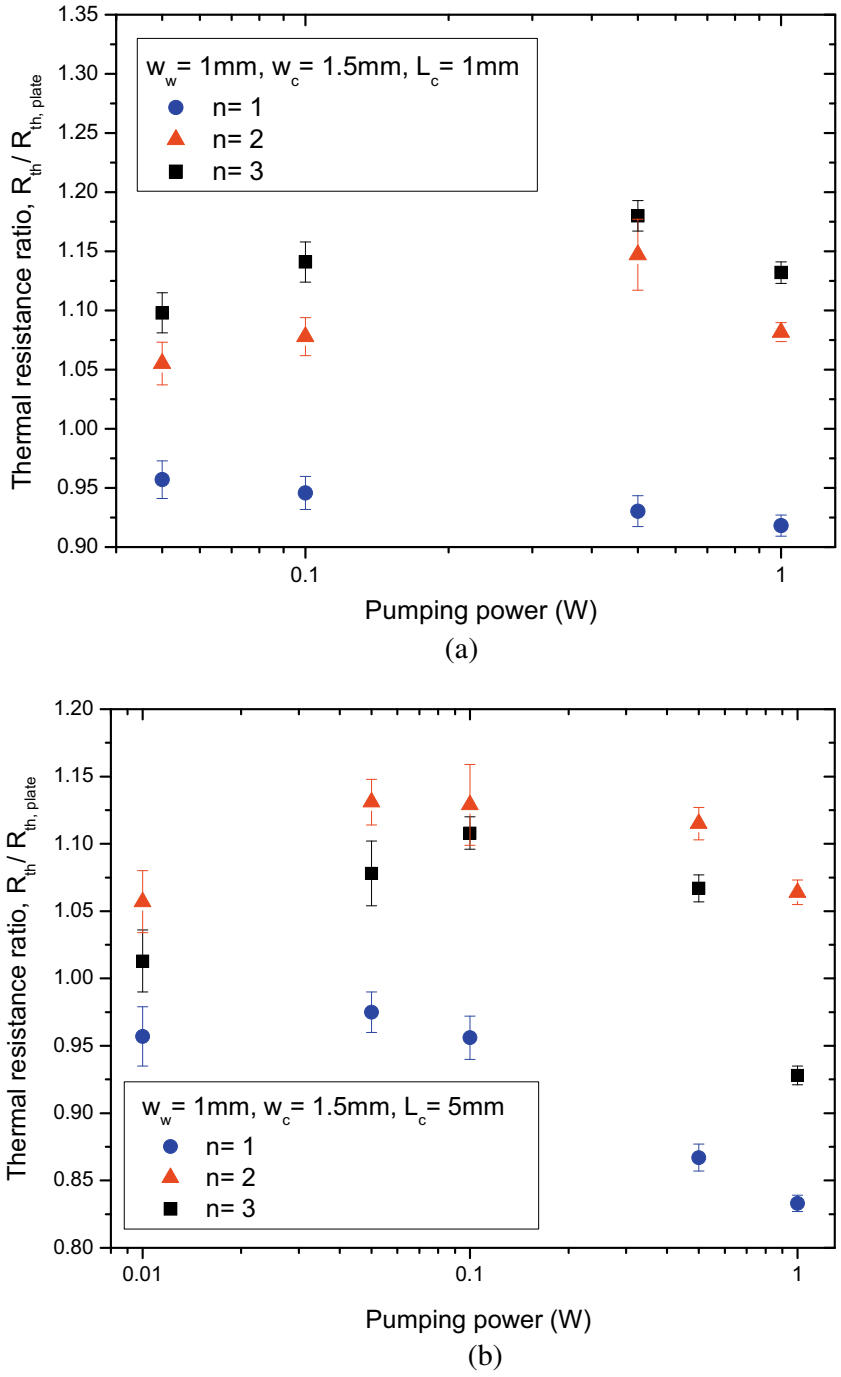

Fig. 8. Effects of the number of cross-cuts on the thermal performance of heat sinks: (a) a length of cross-cut = 1 mm and (b) a length of cross-cut = 5 mm.

When the dimensionless length of a cross-cut becomes zero, the empirical coefficients α, β, γ and δ converge to zero. In this case, the friction factor and the Nusselt number correlations for single-cross-cut heat sinks become those of the plate-fin heat sink. Accordingly, it is clear that Eqs. (3)–(11) are consistent with the equations proposed in Ref. [23,24] regarding a plate-fin heat sink. Eqs. (3)–(11) are applicable for calculating the friction factor and the Nusselt number of cross-cut heat sinks when $0.5 < \varepsilon < 0.71$ and $0 < L_c^* < 0.17$. The optimum value of the thermal resistances and design parameters are obtained from the proposed correlations based on the heat sink size and pumping power range that are used for the experiments, as shown in Table 2. The optimum cross-cut length is approximately 5 mm and the optimum ratio of channel width to fin pitch (ε) is approximately 0.6 for a single-cross-cut heat sink with a length of 60 mm under a parallel flow condition.

3.4. Contour map

Through the use of the proposed correlations for single-cross-cut heat sinks, the thermal performance of single-cross-cut heat sinks was compared to those of optimized plate-fin and square pin-fin heat sinks under the constant pumping power condition. The constant pumping power condition implies that the power required to drive the air through each heat sink is identical. Once the pumping power and the heat sink size are given, optimized

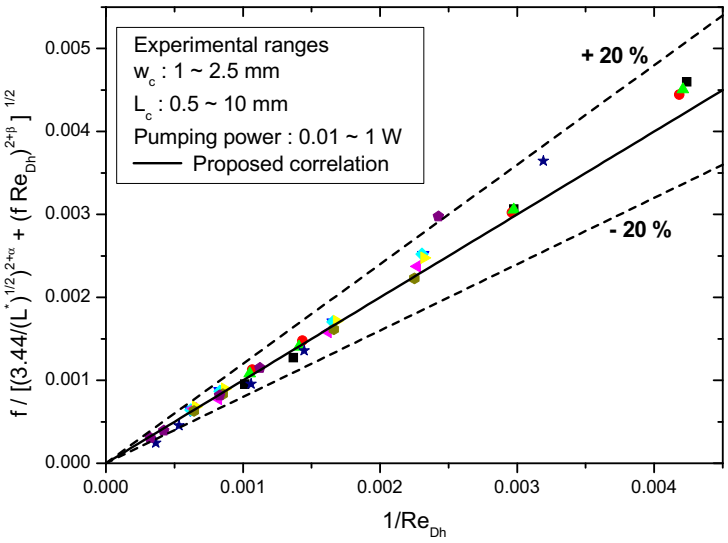

Fig. 9. Validation of the proposed friction factor correlation.

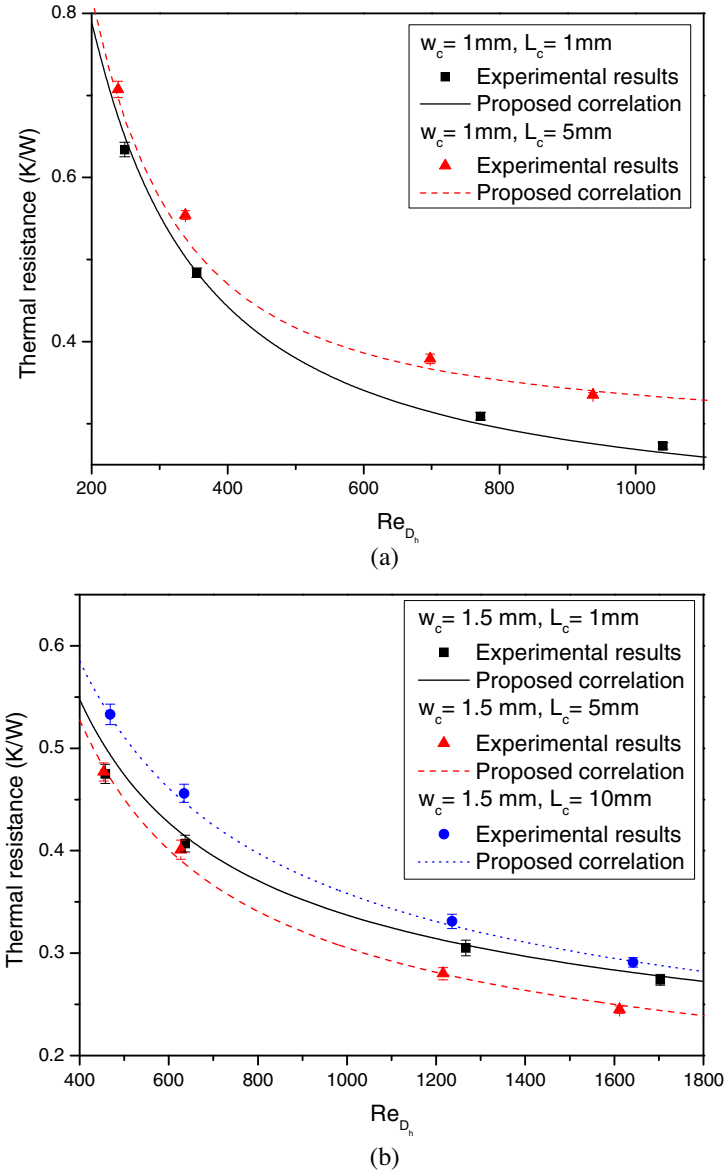

Fig. 10. Validation of the proposed Nusselt number correlation: (a) channel width = 1 mm and (b) channel width = 1.5 mm.

Table 2
Thermal resistances and design parameters for optimized single cross-cut heat sinks.

Pumping power, P_p (W)	Heat sink length, L (mm)	Fin thickness, w_w (mm)	Channel width, w_c (mm)	Cross-cut length, L_c (mm)	Optimum thermal resistance, R (K/W)
0.01	60	1.67	2.54	4.59	0.624
0.05		1.27	1.92	4.56	0.387
0.5		1.13	1.71	4.55	0.317
0.1		0.86	1.3	4.51	0.206
1		0.77	1.16	4.49	0.173

$\left(\rho_f = 1.1774\ \text{kg/m}^3,\ \mu_f = 1.8462 \times 10^{-5}\ \text{kg/m s},\ c_f = 1.0057 \times 10^3\ \text{J/kg K},\ k_f = 0.02624\ \text{W/m K},\ k_s = 171\ \text{W/m K}\right)$.

thermal resistances for each type of heat sink are calculated using the existing and the proposed correlations. For the optimization, the correlations suggested by Muzychka and Yovanovich [23] and Teertstra et al. [24] are used to calculate the friction factor and the Nusselt number of the plate-fin heat sink, respectively. Correlations suggested by Kim et al. [14] are used for the pin-fin heat sink, and the correlations proposed in the present study are used for the cross-cut heat sink. The results obtained from the comparison are presented in a contour map as a function of the dimensionless pumping power and heat sink length. The pumping power range for the experiments, 0.01 W $< P_p <$ 1 W, includes the range of dimensionless pumping power presented in the contour map. The logarithm of the dimensionless length of a heat sink, $\log L^*$ $(\equiv \log(L/D_{h,fr}))$, for the experiments is close to 0.2. Fig. 11(a) and (b) shows the thermal resistance ratio of optimized cross-cut heat sinks and optimized plate-fin heat sink as well as that of optimized cross-cut heat sink and optimized pin-fin heat sink, respectively. By putting together these figures, a contour map for heat sink selection is obtained. As shown in Fig. 11(c), when the dimensionless pumping power is small and the dimensionless heat sink length is large, the plate-fin heat sink is recommended as an optimum heat sink type. However, in the region where the dimensionless pumping power is large and the dimensionless length of the heat sink is small, an optimized pin-fin heat sink is recommended. There is also a region in which the optimized cross-cut heat sink is recommended as an optimum type of heat sink. The region for optimized cross-cut heat sinks lies between the regions for optimized plate-fin and optimized pin-fin heat sinks. As a result, the contour map shows that an optimized single-cross-cut heat sink outperforms optimized plate-fin and square pin-fin heat sinks in the range of $0.04 < \log L^* < 1$.

4. Conclusions

In this study, the effects of the cross-cut on the thermal performance of heat sinks are experimentally investigated under the parallel flow condition. Experimental results show that the cross-cut length primarily influences the thermal performance of heat sinks among all of the design parameters of the cross-cut. The results also show that single-cross-cut heat sinks are superior to multiple-cross-cut heat sinks in the thermal performance under the parallel flow condition. Based on the experimental results, the friction factor and Nusselt number correlations are suggested for single-cross-cut heat sinks. Using the proposed correlations, the thermal performance of optimized single-cross-cut heat sinks is compared to those of optimized plate-fin and square pin-fin heat sinks under the constant pumping power condition. The results obtained from the comparison are presented in a contour map as a function of the dimensionless pumping power and the length of the heat sink. The maximum cooling performance for a given cooling space can be achieved by properly selecting the type of heat sink as well as its detailed dimensions based on the proposed contour map and related correlations, respectively.

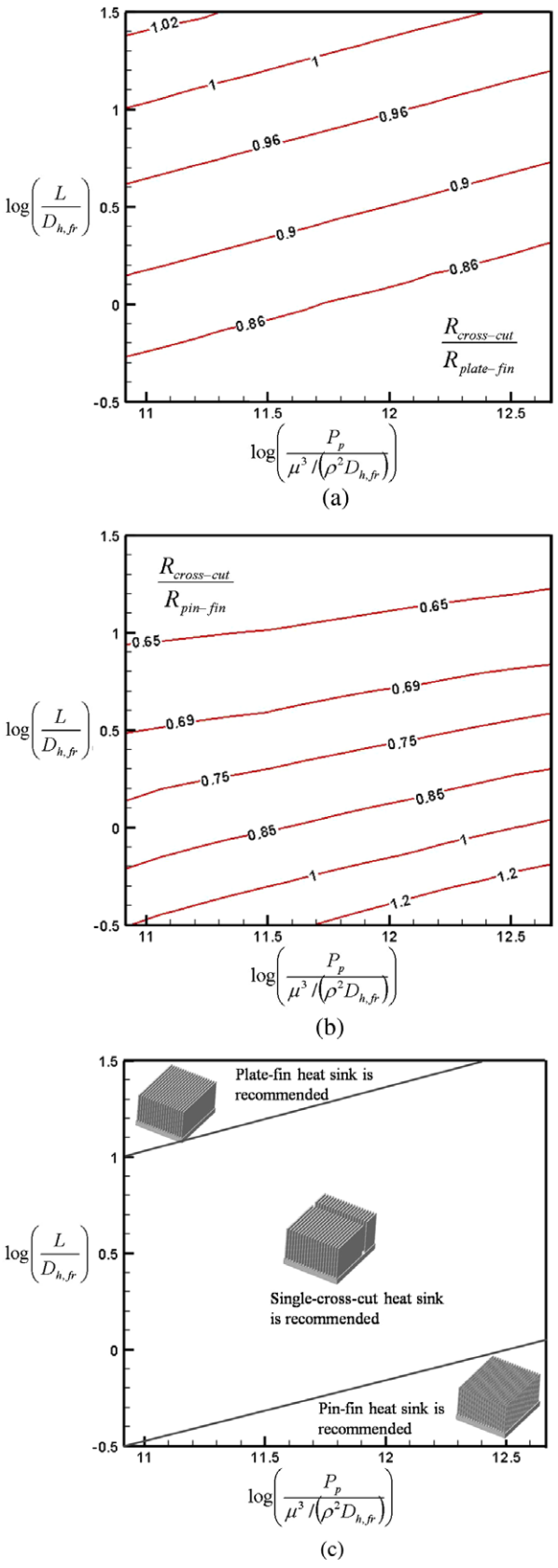

Fig. 11. Contour maps. (a) Comparison of the thermal resistance between the optimized cross-cut and optimized plate-fin heat sinks, (b) comparison of the thermal resistance between the optimized cross-cut and optimized square pin-fin heat sinks and (c) for heat sink selection $\left(\rho_f = 1.1774\ \text{kg/m}^3,\ \mu_f = 1.8462 \times 10^{-5}\ \text{kg/m s},\ c_f = 1.0057 \times 10^3\ \text{J/kg K}, k_f = 0.02624\ \text{W/m K},\ k_s = 171\ \text{W/m K}\right)$.

Acknowledgments

This work was supported by the Korea Science and Engineering Foundation (KOSEF) through the National Research Lab. Program funded by the Ministry of Education, Science and Technology (No. M1060000022406J000022410).

References

[1] F.P. Incropera, Convection heat transfer in electronic equipment cooling, J. Heat Transfer 110 (1988) 1097–1111.
[2] W. Nakayama, Thermal management of electronic equipment: a review of technology and research topics, Appl. Mech. Rev. 39 (12) (1986) 1847–1868.
[3] S. Oktay, R.J. Hannemann, A. Bar-Cohen, High heat from a small package, Mech. Eng. 108 (3) (1986) 36–42.
[4] A. Bar-Cohen, Thermal management of electric components with dielectric liquids, in: J.R. Lloyd, Y. Kurosaki (Eds.), Proceedings of ASME/JSME Thermal Engineering Joint Conference, vol. 2, 1996, pp. 15–39.
[5] D.B. Tuckerman, R.F.W. Pease, High-performance heat sinking for VLSI, IEEE Electron Device Lett. 2 (1981) 126–129.
[6] N.T. Obot, Toward a better understanding of friction and heat/mass transfer in microchannels – a literature review, Microscale Thermophys. Eng. 6 (2002) 155–173.
[7] C.K. Loh, D. Nelson, D.J. Chou, Optimization of Heat Sink Design and Fan Selection in Portable Electronics Environment, Tech. Rep. Available from: <http://www.enertron-inc.com/PDF/Fan%20Heat%20Sink%20optimization.pdf>, 2002.
[8] S.Y. Kim, A.V. Kuznetsov, Optimization of pin-fin heat sinks using anisotropic local thermal non-equilibrium porous model in a jet impinging channel, Numer. Heat Transfer A 44 (8) (2003) 771–787.
[9] G.P. Peterson, C.S. Chang, Heat transfer analysis and evaluation for two-phase flow in porous-channel heat sinks, Numer. Heat Transfer A 31 (2) (1997) 113–130.
[10] S.Y. Kim, J.-M. Koo, A.V. Kuznetsov, Effect of anisotropy in permeability and effective thermal conductivity on thermal performance of an aluminum foam heat sink, Numer. Heat Transfer A 40 (1) (2001) 21–36.
[11] T.-G. Maxime, G. Louis, Thermal resistance minimization of a fin-and-porous-medium heat sink with evolutionary algorithms, Numer. Heat Transfer A 54 (4) (2008) 349–366.
[12] S.Y. Kim, R.L. Webb, Thermal performance analysis of fan-heat sinks for CPU cooling, in: Proceedings of the IMECE'03, IMECE2003-42172, 2003.
[13] D. Kim, S. J. Kim, A. Ortega, Thermal optimization of microchannel heat sink with pin fin structures, in: Proceedings of the IMECE'03, IMECE2003-42180, 2003.
[14] S.J. Kim, D.-K. Kim, H.H. Oh, Comparison of fluid flow and thermal characteristics of plate-fin and pin-fin heat sinks subject to a parallel flow, Heat Transfer Eng. 29 (2) (2008) 169–177.
[15] Y.-T. Yang, H.-S. Peng, Numerical study of thermal and hydraulic performance of compound heat sink, Numer. Heat Transfer A 55 (5) (2009) 432–447.
[16] J.L. Xu, Y.H. Gan, D.C. Zhang, X.H. Li, Microscale heat transfer enhancement using thermal boundary layer developing concept, Int. J. Heat Mass Transfer 48 (9) (2005) 1662–1674.
[17] H. Jonsson, B. Moshfegh, Modeling of the thermal and hydraulic performance of plate fin, strip fin, and pin fin heat sinks-influence of flow bypass, IEEE Trans. Compon. Packag. Technol. 24 (2000) 117–123.
[18] I.E. Idelchik, Flow Resistance, A Design Guide for Engineers, Hemisphere, New York, 1989.
[19] K. Noda, K. Tatsumi, K. Nakabe, Effect of cut-fin shape on heat transfer and pressure loss performance, Natl. Heat Transfer Sympos. Jpn. 3 (2004) 799–800.
[20] C.H. Amon, B.B. Mikic, Numerical prediction of convective heat transfer in self-sustained oscillatory flows, J. Thermophys. 4 (2) (1990) 239–246.
[21] C.H. Amon, D. Majumdar, C.V. Herman, F. Mayinger, B.B. Mikic, D.P. Sekulic, Numerical and experimental studies of self-sustained oscillatory flows in communicating channels, Int. J. Heat Mass Transfer 35 (11) (1992) 3115–3129.
[22] T.G. Beckwith, R.D. Marangoni, J.H. Lienhard, Mechanical Measurement, Addison-Wesley, New York, 1993.
[23] Y.S. Muzychka, M.M. Yovanovich, Modeling friction factors in non-circular ducts for developing laminar flow, in: Proceedings of the second AIAA Theoretical Fluid Mechanics Meeting, Albuquerque, 1998.
[24] P. Teertstra, M.M. Yovanovich, J.R. Culham, Analytical forced convection modeling of plate fin heat sink, in: Proceedings of the 15th IEEE Semi-Thermal Symposium, 1999, pp. 34–41.
[25] D. Kim, S.J. Kim, A. Ortega, Compact modeling of fluid flow and heat transfer in pin fin heat sinks, ASME J. Electron. Packag. 126 (2004) 342–350.
[26] B.R. Munson, D.F. Young, T.H. Okiishi, Fundamentals of Fluid Mechanics, fourth ed., Wiley, New York, 2002 (Chapter 8).